Stem Cell Reports
Article

ISSCR

OPEN ACCESS

Involvement of LIN28A in Wnt-dependent regulation of hippocampal neurogenesis in the aging brain

Zhechun Hu,[1,7] Jiao Ma,[2,7] Huimin Yue,[1] Yujian Luo,[2] Xiaofang Li,[2] Chao Wang,[1] Liang Wang,[3] Binggui Sun,[4,6] Zhong Chen,[5] Lang Wang,[2,*] and Yan Gu[1,6,*]

[1]Center of Stem Cell and Regenerative Medicine and Department of Neurology of the Second Affiliated Hospital, NHC and CAMS Key Laboratory of Medical Neurobiology, Zhejiang University School of Medicine, Hangzhou 310058, China
[2]Department of Neurology of the First Affiliated Hospital, Interdisciplinary Institute of Neuroscience and Technology, Zhejiang University School of Medicine, Hangzhou 310029, China
[3]Institute of Neuroscience and Department of Neurology of the Second Affiliated Hospital, Mental Health Center, NHC and CAMS Key Laboratory of Medical Neurobiology, Zhejiang University School of Medicine, Hangzhou 310058, China
[4]NHC and CAMS Key Laboratory of Medical Neurobiology, School of Brain Science and Brain Medicine, Zhejiang University, Hangzhou 310058, China
[5]Key Laboratory of Neuropharmacology and Translational Medicine of Zhejiang Province, School of Pharmaceutical Sciences, Zhejiang Chinese Medical University, Hangzhou 310053, China
[6]MOE Frontier Science Center for Brain Science & Brain-Machine Integration, Zhejiang University, Hangzhou 310058, China
[7]These authors contributed equally
*Correspondence: wanglang@zju.edu.cn (L.W.), guyan2015@zju.edu.cn (Y.G.)
https://doi.org/10.1016/j.stemcr.2022.05.016

SUMMARY

Hippocampal neurogenesis declines with aging. Wnt ligands and antagonists within the hippocampal neurogenic niche regulate the proliferation of neural progenitor cells and the development of new neurons, and the changes of their levels in the niche mediate aging-associated decline of neurogenesis. We found that RNA-binding protein LIN28A remained existent in neural progenitor cells and granule neurons in the adult hippocampus and that it decreased with aging. *Lin28a* knockout inhibited the responsiveness of neural progenitor cells to niche Wnt agonists and reduced neurogenesis, thus impairing pattern separation. Overexpression of *Lin28a* increased the proliferation of neural progenitor cells, promoted the functional integration of newborn neurons, restored neurogenesis in Wnt-deficient dentate gyrus, and rescued the impaired pattern separation in aging mice. Our data suggest that LIN28A regulates adult hippocampal neurogenesis as an intracellular mechanism by responding to niche Wnt signals, and its decrease is involved in aging-associated decline of hippocampal neurogenesis and related cognitive functions.

INTRODUCTION

In the adult mammalian hippocampus, neural progenitor cells (NPCs) in the subgranular zone (SGZ) of the dentate gyrus (DG) give rise to newborn neurons throughout life (Ming and Song, 2011). Continuously generated newborn neurons integrate into the existing neural circuits and play essential roles for hippocampal functions (Anacker and Hen, 2017; Christian et al., 2014; Goncalves et al., 2016).

Accumulating evidence indicates that the hippocampal neurogenesis decreases with aging (Kuhn et al., 1996; Ngwenya et al., 2015; Spalding et al., 2013), which is believed to be associated with declines in hippocampal-dependent cognitive functions (Seib et al., 2013). It is reported that Wnt ligands and antagonists, which are secreted by local astrocytes and/or neurons in the hippocampal neurogenic niche, regulate both the proliferation of NPCs and the development of new neurons (Jang et al., 2013; Kuwabara et al., 2009; Lie et al., 2005; Song et al., 2002). Decreased Wnt ligands production and enhanced Wnt antagonists secretion in the DG are associated with aging, leading to decreased canonical Wnt signaling and reduced neurogenesis (Bayod et al., 2015; Heppt et al., 2020; Miranda et al., 2012; Okamoto et al., 2011; Seib et al., 2013). However, the intracellular mechanisms underlying Wnt-related regulation of neurogenesis have not been fully revealed.

LIN28 is an RNA-binding protein regulating self-renewal of embryonic stem cells and a variety of biological processes (Shyh-Chang and Daley, 2013). In the developing mammalian nervous system, LIN28 homolog A (*Lin28a*) is highly expressed in the NPCs during early embryonic stages, regulating the brain development (Balzer et al., 2010; Yang et al., 2015). Recent studies showed that LIN28A remains in NPCs in the adult brain and retina (Cimadamore et al., 2013; Yao et al., 2016), raising the possibility that LIN28A may regulate neurogenesis in the adult or even aging brain.

In this study, we provided evidence that LIN28A exists in NPCs and neurons in the adult DG and declines with aging. We found that LIN28A regulated the proliferation of NPCs and the development of newborn neurons as an intracellular mechanism downstream of Wnt signaling. Thus, responding to the aging-associated changes of Wnt ligands/inhibitors in the SGZ, the decrease of *Lin28a* expression leads to the decline of hippocampal neurogenesis. Increasing the expression of *Lin28a* in hippocampal

NPCs in aging mice could rescue their neurogenesis and related cognitive functions.

RESULTS

Lin28a expression in the DG of adult brain decreased with aging

We first examined the presence of LIN28 in the DG of the adult mouse brain. Using RNAscope in brain sections from adult Nestin-GFP mice, we found that *Lin28a*, but not *Lin28b*, mRNA signals existed in the granule cell layer (GCL) compared with the signals obtained using negative control (Neg-ctrl) or positive control (Pos-ctrl) probes (Figure 1A). Specifically, *Lin28a* mRNA colocalized with the cell bodies of Nestin$^+$ NPCs and PROX1$^+$ dentate granule cells (DGCs) (Figure 1B).

We next performed immunohistochemistry and observed LIN28A protein in the GCL of the DG (Figure S1A). Consistently, LIN28A was found in Nestin$^+$ NPCs and PROX1$^+$ DGCs (Figure 1C). In contrast, in Nestin-Cre::*Lin28a*$^{f/f}$ mice (*Lin28a*$^{f/f}$), LIN28A was not detected in either the GCL or the SGZ (Figure S1B).

Interestingly, we found LIN28A protein levels in the DG decreased in aging mice (14 months old, 14 mo) compared with young adult mice (2 months old, 2 mo) (Figures 1D and 1E). Using RNAscope, we found that the number of dots marked by *Lin28a* mRNA probes in each cell, reflecting its expression level, became significantly less in 14-month-old mice compared with 2-month-old mice in both Nestin$^+$ NPCs (Figures 1F and 1G) and PROX1$^+$ DGCs (Figures 1H and 1I), indicating an aging-associated decrease of *Lin28a* expression in these cells.

LIN28A in hippocampal NPCs was essential for neurogenesis and pattern separation

To find out whether the decrease of *Lin28a* expression in the DG is related to cognitive declines in aging animals, we trained young adult (2 months old) and aging (10 months old) mice for a series of behavior tests. We found that the 10-month-old mice showed decreased novel-location recognition (NLR) (Figure S2A), while the novel-object recognition (NOR) was not affected (Figure S2B). The 2- and 10-month-old mice did not show significant differences in single-trial contextual fear conditioning (CFC) tests (Figure S2C). However, when we used a pattern-separation paradigm (Figure 2A) as previously reported (Sahay et al., 2011a), we found that the 10-month-old mice discriminated the two similar contexts A and B in session 6 much later than the 2-month-old mice, which showed discrimination in session 4 (Figure 2B). This result suggested that aging is associated with a decreased ability of pattern separation. Furthermore, when tested in an open field (OF), the 10-month-old mice showed less time spent in the center zone than the 2-month-old mice (Figure S2D), indicating that the aging mice had higher anxiety levels.

Pattern separation is believed to be one of the hippocampal functions most related to neurogenesis (Sahay et al., 2011b). Indeed, the 10-month-old mice showed significantly less doublecortin (DCX)-positive cells in the DG (Figures S2E and S2F), indicating an aging-associated decline of hippocampal neurogenesis (Seib et al., 2013).

To test whether LIN28A is related to adult neurogenesis, we knocked out *Lin28a* from Nestin$^+$ NPCs in Nestin-Cre^{ERT2}::*Lin28a*$^{f/f}$ mice by tamoxifen (TAM) treatment (Figure 2C). Four weeks later, we found that *Lin28a* knockout (KO) from NPCs significantly decreased the density and percentage of cells expressing proliferation marker minichromosome maintenance complex component 2 (MCM2) in the GCL (Figures 2D–2F). Similarly, DCX$^+$ cells significantly decreased in the DG of the TAM-treated mice compared with vehicle (Veh)-treated mice (Figures 2G–2I). To further verify whether NPCs lacking LIN28A indeed produces fewer new neurons, we treated Nestin-Cre^{ERT2}::*Lin28a*$^{f/f}$::Ai14 (*Lin28a*$^{f/f}$) mice with TAM, while using Nestin-Cre^{ERT2}::*Lin28a*$^{+/+}$::Ai14 mice of the same age and genetic background as Ctrl, and examined the number of dTomato$^+$ cells in the DG 6 weeks later (Figure 2J). We found that *Lin28a* KO indeed decreased the density and proportion of dTomato$^+$ cells in the DG (Figures 2K–2M). However, the proportion of NeuN$^+$ DGCs in the dTomato$^+$ cells was not altered (Figures S3A and S3B). These data suggest that LIN28A is necessary for the generation of new neurons from NPCs, whereas loss of *Lin28a* leads to decreased neurogenesis in the adult DG.

We then tested Nestin-Cre^{ERT2}::*Lin28a*$^{f/f}$ mice for pattern separation 6 weeks after Veh/TAM treatment (Figure 2N). Consistent with the decreased hippocampal neurogenesis, TAM-treated mice discriminated contexts A and B later than Veh-treated mice (Figure 2O), mimicking the decreased ability of pattern separation in aging animals.

In addition, similar to the behavioral phenotypes seen in the aging animals, TAM-treated Nestin-Cre^{ERT2}::*Lin28a*$^{f/f}$ mice did not show significant differences in single-trial CFC (Figure S3C) or NOR tests (Figure S3D). However, TAM-treated mice showed impaired NLR tests (Figure S3E) and exhibited enhanced anxiety in the OF test (Figure S3F).

These results suggest that the decreased *Lin28a* expression in hippocampal NPCs may contribute to the decline of neurogenesis and the cognitive defects in aging animals.

Lin28a overexpression increased the progenies of NPCs in the adult DG

Next, to investigate how LIN28A regulates NPCs in the adult brain, we generated FLEX retroviral vectors that express GFP (Ctrl) or GFP-p2A-*Lin28a* (*Lin28a*-OE) (Figure

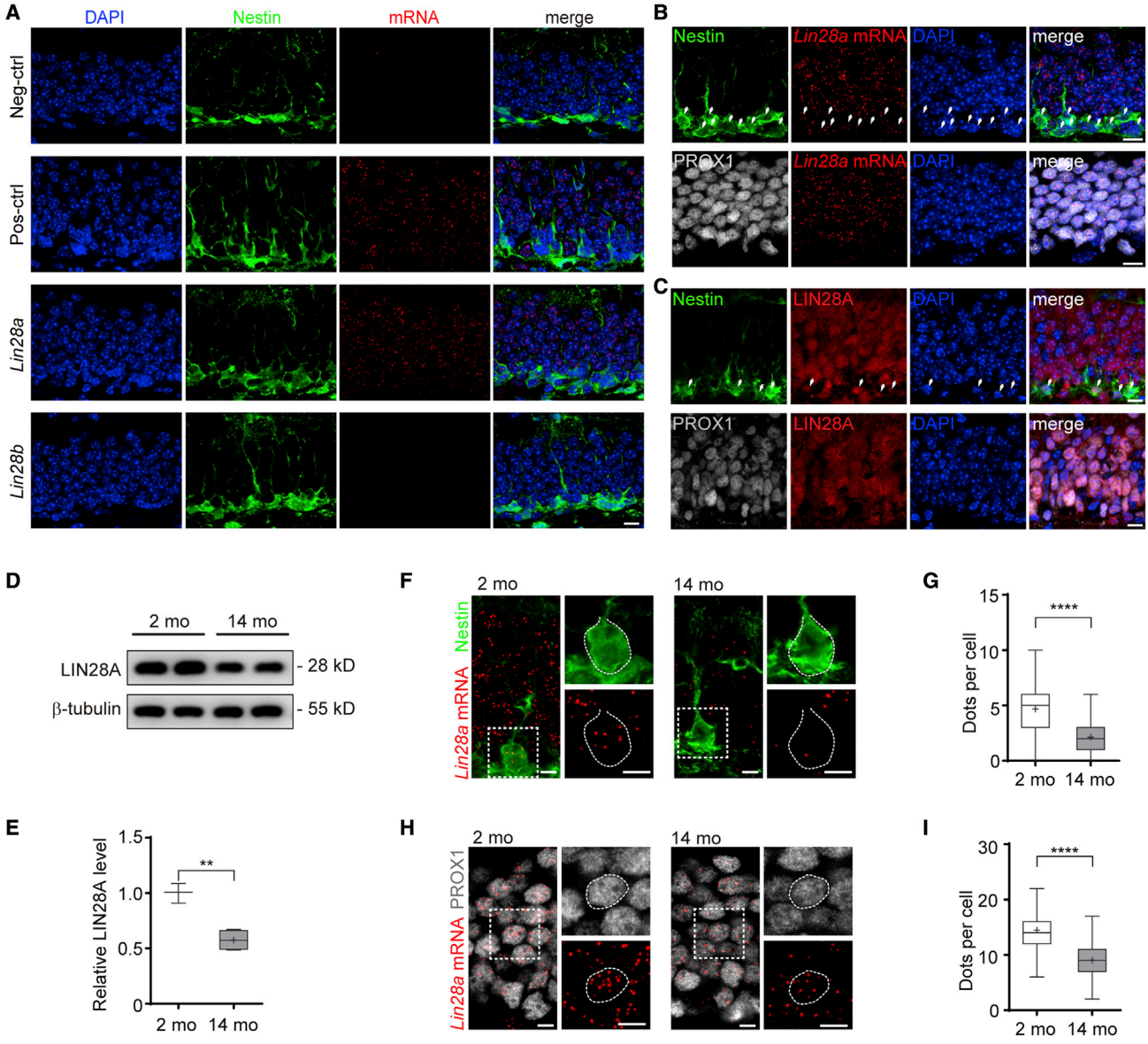

Figure 1. Expression of *Lin28a* in the DG of adult brain decreases with age

(A) RNAscope images from Nestin-GFP mouse brain sections, with Neg-ctrl, Pos-ctrl, *Lin28a*, and *Lin28b* probes. Scale bar: 20 μm.

(B) RNAscope images showing *Lin28a* mRNA in Nestin$^+$ NPCs (top) and PROX1$^+$ DGCs (bottom) in the DG. White arrows indicate *Lin28a* mRNA in Nestin$^+$ NPCs. Scale bars: 10 μm.

(C) Top panel: images showing LIN28A in Nestin$^+$ NPCs (top) and PROX1$^+$ DGCs (bottom) in the DG of adult Nestin-GFP mice. White arrows indicate LIN28A in Nestin$^+$ NPCs. Scale bars: 10 μm.

(D and E) Western blotting showing LIN28A level in the DG of 2- and 14-month-old mice. β-tubulin was used as the internal control (2-month-old n = 3 mice, 14-month-old n = 4 mice, **p = 0.0016).

(F) RNAscope images showing *Lin28a* mRNA in Nestin$^+$ NPCs in 2- and 14-month-old mice. Scale bars: 5 μm.

(G) Number of *Lin28a* mRNA dots in each Nestin$^+$ NPC (2-month-old N = 3 mice, n = 82 cells; 14-month-old N = 3 mice, n = 90 cells; ****p < 0.0001).

(H) RNAscope images showing *Lin28a* mRNA in PROX1$^+$ DGCs. Scale bar: 5 μm.

(I) Number of *Lin28a* mRNA dots in each PROX1$^+$ DGC (2-month-old N = 3 mice, n = 99 cells; 14-month-old N = 3 mice, n = 111 cells; ****p < 0.0001).

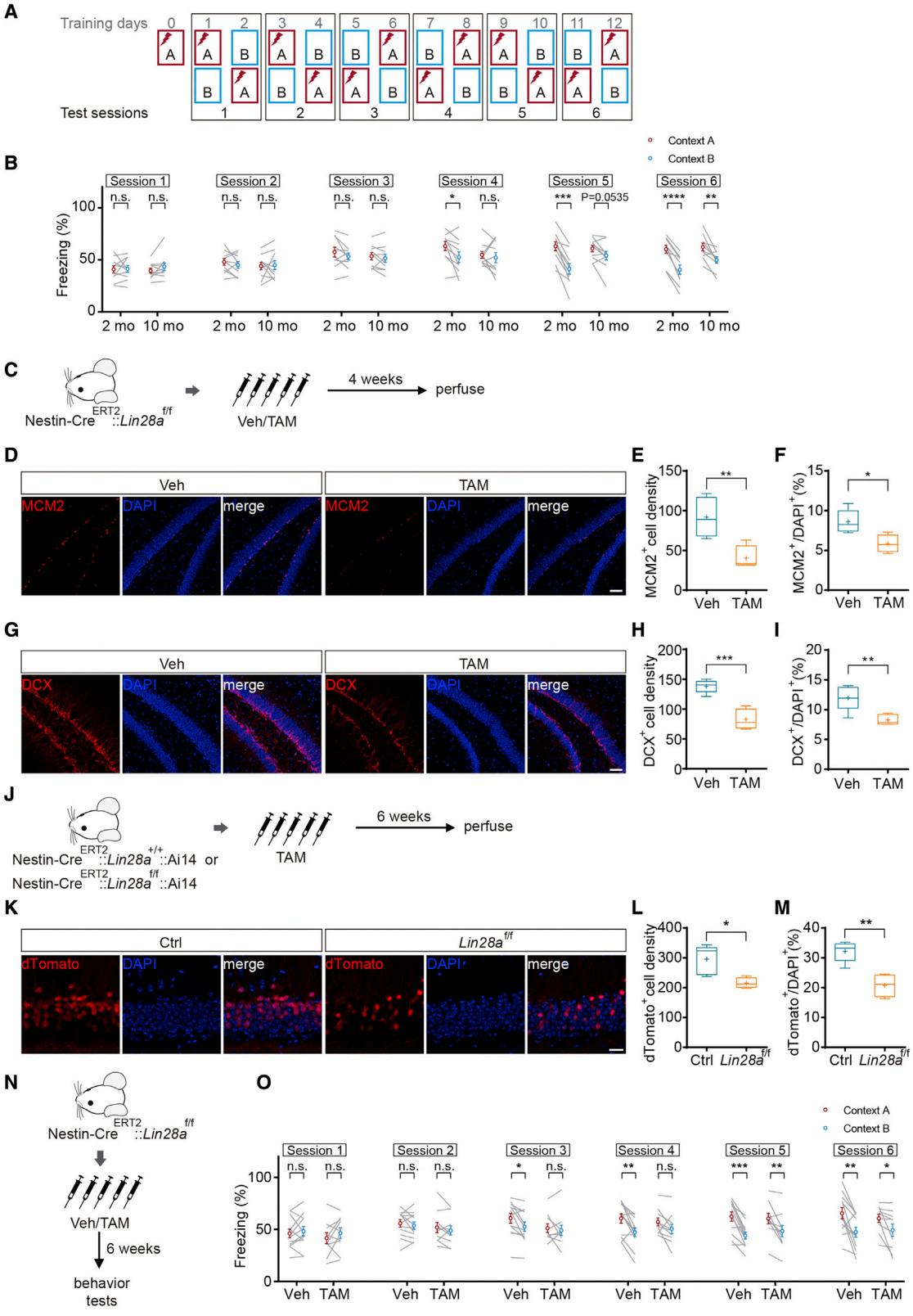

(legend on next page)

3A). We injected diluted virus into the DG of adult Nestin-Cre mice to sparsely label individual dividing Nestin$^+$ NPCs and their progenies (Figure 3B). We examined GFP$^+$ cell clusters 7 days post viral injection (dpi) and found that *Lin28a* overexpression (OE) significantly increased the cluster size, from an average of 1.77 ± 0.11 to 3.23 ± 0.26 cells per cluster (Figures 3C–3E).

To avoid possible mixture of adjacently labeled clusters, we designed a FLEX m/n/cXFP retroviral reporter system that expresses membranous RFP (mRFP), nuclear CFP (nCFP), or cytosolic GFP (cGFP) in random combinations depending on Cre recombinase (Figure 3F). Consistently, 7 dpi in Nestin-Cre mice, cells overexpressing *Lin28a* (containing cGFP) exhibited an increased cluster size of 2.73 ± 0.18 cells compared with 1.48 ± 0.08 cells in Ctrl clusters (Figures 3G–3I), confirming that *Lin28a* OE did increase the number of cells generated from each NPC.

To investigate how LIN28A regulates the number of progenies of NPCs, we tested whether Lin28a could regulate the cell cycle of hippocampal NPCs. Two dpi of FLEX retroviruses (Figure 3A) into the DG of Nestin-Cre mice, we treated the animals with BrdU every 6 h for 5 times. We perfused the mice at 7 dpi and stained the brain sections for BrdU and MCM2 (Figure 3J). By this method, we could label dividing Nestin$^+$ NPCs with GFP at their first division and then mark their second division with BrdU if the mitosis happened during the window of BrdU administration, while a third division could be detected by MCM2 staining (Figure 3K). We found that *Lin28a* OE significantly increased the percentage of GFP$^+$BrdU$^+$ and GFP$^+$BrdU$^+$MCM2$^+$ cells in GFP$^+$ cells (Figure 3L), indicating that *Lin28a* OE increased the cell cycles of NPCs. To confirm this result, we stained for an M-phase marker phosphor-H3 (pH3), instead of MCM2, which marks the S phase of the cell cycle (Figures S4A and S4B). Consistently, we found that *Lin28a* OE increased GFP$^+$BrdU$^+$ and GFP$^+$BrdU$^+$pH3$^+$ cells in GFP$^+$ cells (Figure S4C). These results indicate that *Lin28a* OE enlarges the size of cell clusters via increasing the cell cycles of NPCs and their progenies.

As adult hippocampal NPCs go through several stages to produce new neurons (Ming and Song, 2011), we next characterized the effects of *Lin28a* OE on different stages of neurogenesis. Seven days after tagging dividing NPCs using FLEX retroviruses in Nestin-Cre mice, we stained for markers to examine the stages of GFP$^+$ cells. We used GFAP$^+$S100β$^-$ as a marker for type 1 radial glia-like precursor cells (Figure S4D), ASCL1$^+$ for early type 2a cells (Figure S4E), TBR2$^+$ for late type 2a/type 2b cells (Figure S4F), and DCX$^+$ for type 3 neuroblasts/immature neurons (Figure S4G). Our results showed that *Lin28a* OE did not significantly alter the proportion of GFAP$^+$S100β$^-$, ASCL1$^+$, DCX$^+$ subpopulations in GFP$^+$ cells but did increase the proportion of TBR2$^+$ cells (Figure S4H), suggesting that *Lin28a* OE may increase neurogenesis by expanding the type 2 intermediate progenitor cells. In addition, we found that *Lin28a* OE decreased the percentage of S100β$^+$ cells (Figures S4I and S4J), suggesting that LIN28A may potentially inhibit the differentiation of newborn cells toward astrocytes.

Figure 2. LIN28A is necessary for adult hippocampal neurogenesis and pattern separation

(A) Experimental schematics for testing pattern separation in mice.

(B) Freezing of 2- and 10-month-old mice in contexts A and B in test sessions 1 through 6 (2-month-old n = 10 mice, 10-month-old n = 10 mice; two-tailed paired t test; session 1: 2-month-old p = 0.8886, 10-month-old p = 0.1421; session 2: 2-month-old p = 0.3272, 10-month-old p = 0.8362; session 3: 2-month-old p = 0.1976, 10-month-old p = 0.4024; session 4: 2-month-old *p = 0.0255, 10-month-old p = 0.5356; session 5: 2-month-old ***p = 0.0001, 10-month-old p = 0.0535; session 6: 2-month-old ****p < 0.0001, 10-month-old **p = 0.0036).

(C) Paradigm showing *Lin28a* KO from Nestin$^+$ NPCs.

(D) Images showing MCM2$^+$ cells in the SGZ. Scale bar: 50 μm.

(E and F) *Lin28a* KO decreased the density (Veh n = 5 mice, TAM n = 4 mice; **p = 0.0083) and the percentage of MCM2$^+$ cells in the GCL (Veh n = 5 mice, TAM n = 4 mice; *p = 0.0158).

(G) Images showing DCX$^+$ cells in the DG. Scale bar: 50 μm.

(H and I) *Lin28a* KO decreased the density (Veh n = 5 mice, TAM n = 5 mice; ***p = 0.00023) and the percentage of DCX$^+$ cells in the DG (Veh n = 5 mice, TAM n = 5 mice; **p = 0.0064).

(J) Experimental schematics.

(K) dTomato$^+$ cells in the GCL. Scale bar: 20 μm.

(L and M) *Lin28a* KO decreased the density (Ctrl n = 5 mice, *Lin28a*$^{f/f}$ n = 4 mice; *p = 0.0170) and the percentage of dTomato$^+$ cells in the GCL (Ctrl n = 5 mice, *Lin28a*$^{f/f}$ n = 4 mice; **p = 0.0020).

(N) Experimental schematics.

(O) Freezing of Veh- and TAM-treated mice in contexts A and B in test sessions 1 through 6 (Veh n = 12 mice, TAM n = 10 mice; two-tailed paired t test; session 1: Veh p = 0.5156, TAM p = 0.2795; session 2: Veh p = 0.3921, TAM p = 0.2694; session 3: Veh *p = 0.0153, TAM p = 0.5583; session 4: Veh **p = 0.0057, TAM p = 0.0863; session 5: Veh ***p = 0.0002, TAM **p = 0.0075; session 6: Veh **p = 0.0047, TAM *p = 0.0281).

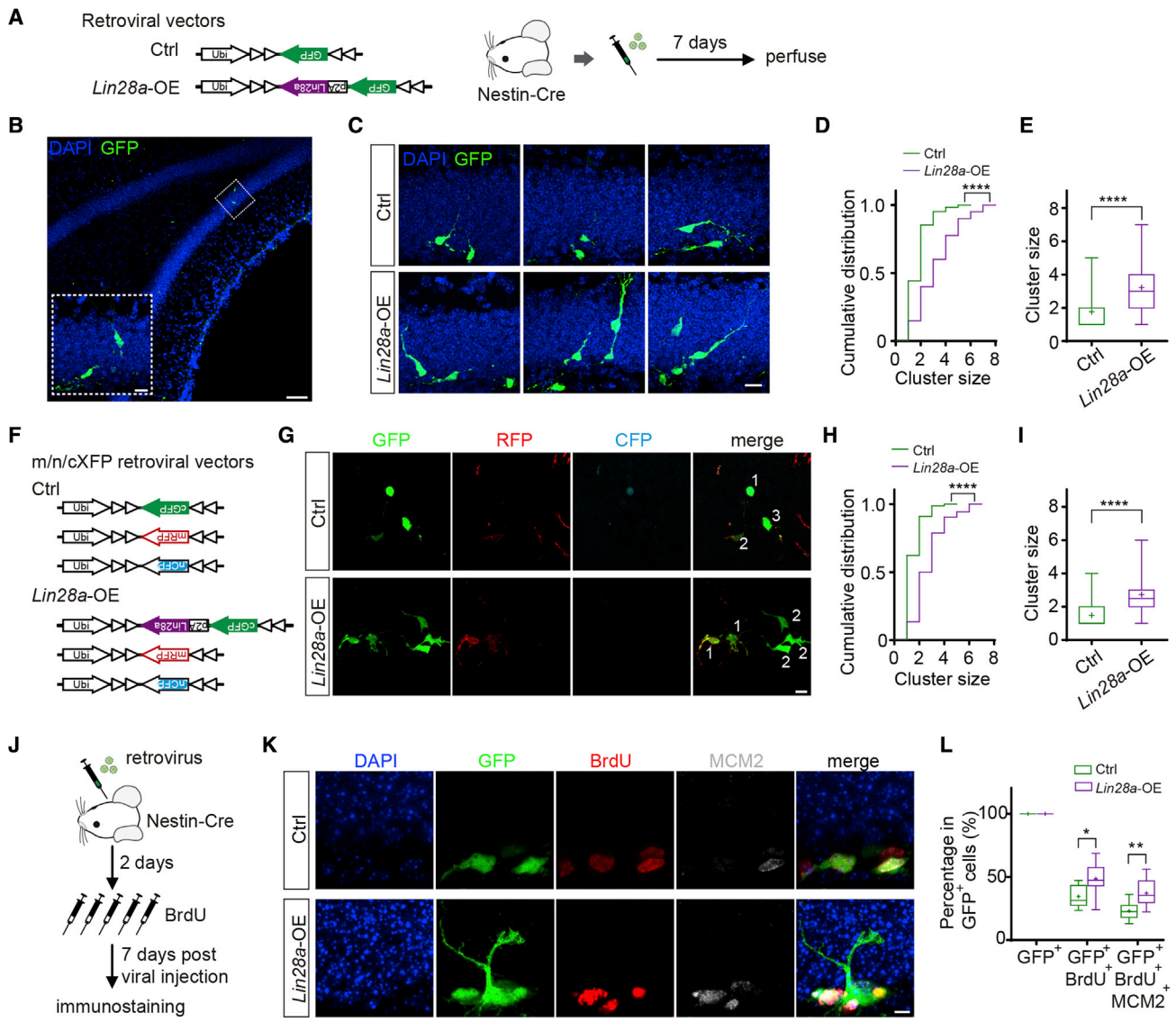

Figure 3. *Lin28a* OE increases the progenies of individual NPCs

(A) FLEX retrovirus was injected into the DG of Nestin-Cre mice.

(B) Image showing the sparse labeling of an individual cluster of newborn cells in the DG. Scale bar: 50 μm. Inset shows an enlarged image of the 2-cell cluster in the square area marked by dotted line. Scale bar: 10 μm.

(C) Cell clusters labeled by Ctrl or *Lin28a*-OE retroviruses. Scale bar: 10 μm.

(D) Cumulative distribution of cell cluster size (Ctrl N = 11 mice, n = 61 clusters; *Lin28a*-OE N = 8 mice, n = 40 clusters; Kolmogorov-Smirnov test, ****$p < 0.0001$).

(E) The average size of cell clusters (Ctrl n = 61 clusters; *Lin28a*-OE n = 40 clusters; ****$p < 0.0001$).

(F) FLEX m/n/cXFP retroviral vectors.

(G) Images showing cell clusters labeled by Ctrl or *Lin28a*-OE combination of retroviruses. Different numbers indicate different clusters. Scale bar: 10 μm.

(H) Cumulative distribution of cell-cluster sizes (Ctrl N = 8 mice, n = 77 clusters; *Lin28a*-OE N = 7 mice, n = 52 clusters; Kolmogorov-Smirnov test, ****$p < 0.0001$).

(I) The average size of cell clusters. (Ctrl N = 8 mice, n = 77 clusters; *Lin28a*-OE N = 7 mice, n = 52 clusters; ****$p < 0.0001$).

(J) Experimental scheme for analyzing the cell cycles *in vivo*.

(K) Images showing GFP^+ cells colocalizing with BrdU and/or MCM2. Scale bar: 5 μm.

(L) *Lin28* OE increased the percentage of GFP^+BrdU^+ cells (Ctrl n = 10 mice, *Lin28a*-OE n = 8 mice, *$p = 0.0142$) and $GFP^+BrdU^+MCM2^+$ cells (Ctrl n = 10 mice, *Lin28a*-OE n = 8 mice, **$p = 0.0040$) in GFP^+ cells.

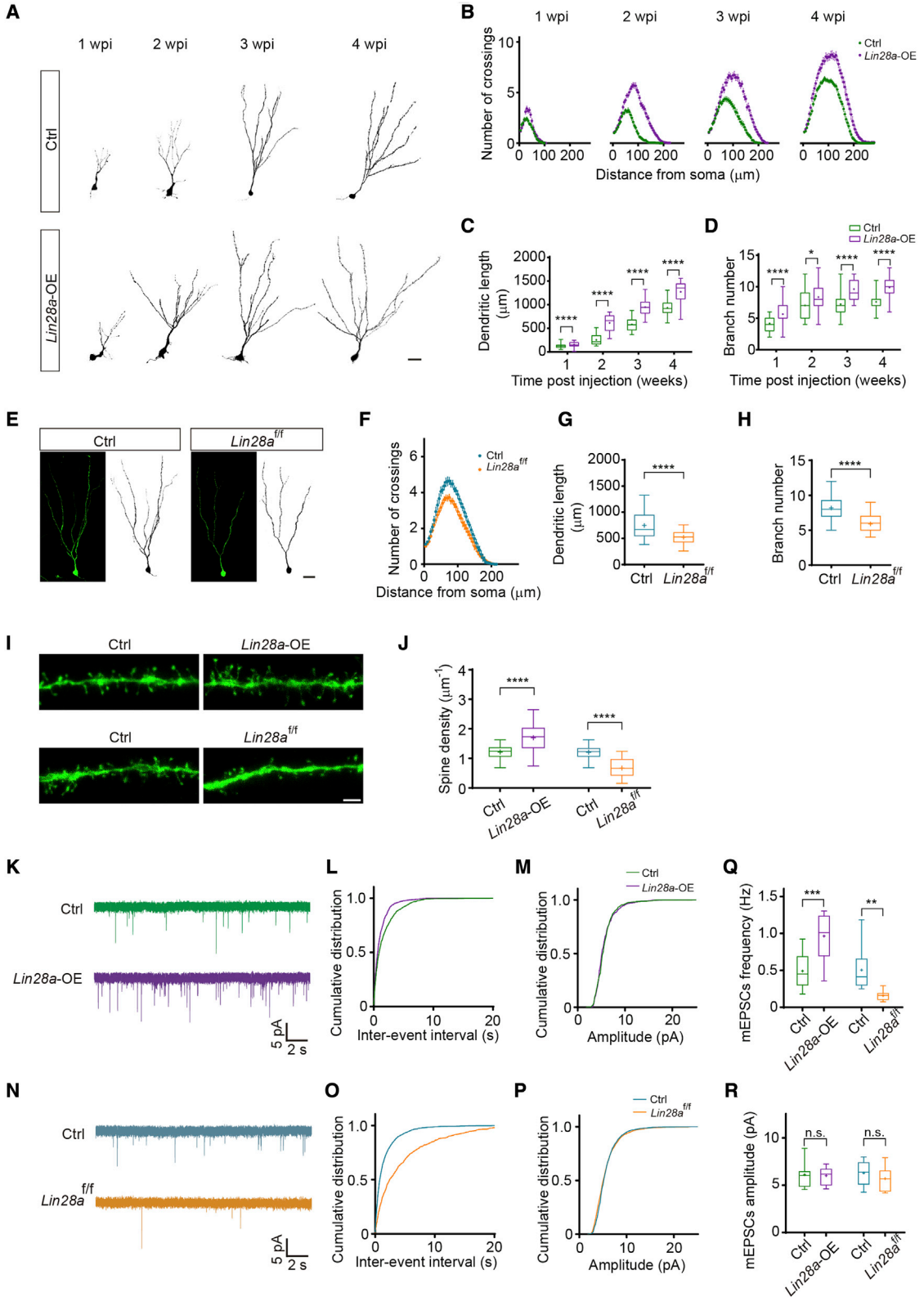

(legend on next page)

As a majority of the newborn cells undergo apoptosis during the first week after cell birth (Sierra et al., 2010), we next stained for activated caspase-3 (aCas-3) at 4 dpi (Figure S4K). We did not find that *Lin28a* OE altered the colocalization of aCas-3 with GFP$^+$ newborn cells (Figure S4L).

LIN28 regulates multiple downstream effectors by repressing *let-7* biogenesis (Shyh-Chang and Daley, 2013). To test whether LIN28A regulates neurogenesis through *let-7*-dependent pathways, we constructed a retrovirus expressing a *let-7* sponge to directly inhibit *let-7* (Figure S5A), as previously described (Yang et al., 2012). After coinjection with pUX-FLEX-mRFP in Nestin-Cre mice, we examined the GFP$^+$RFP$^+$ cell clusters (Figure S5B) and found that *let-7* sponge significantly increased the cluster size (Figures S5C and S5D), mimicking the pro-neurogenic effects of *Lin28a* OE. This suggested that Lin28a regulated the proliferation of NPCs and their progenies through *let-7*-dependent mechanisms.

LIN28A regulated the development and functional integration of new neurons in the adult DG

Since LIN28A was also detected in DGCs, we wondered whether LIN28A regulates the development and functional integration of the new neurons. We labeled the newborn DGCs in adult C57BL/6 mice using retroviruses expressing GFP (Ctrl) or GFP-p2A-*Lin28a* (*Lin28a*-OE) and examined the morphological development of GFP$^+$ neurons at 1, 2, 3, and 4 weeks post retroviral injection (wpi) (Figure 4A). Our data showed that neurons overexpressing *Lin28a* exhibited more complex dendrites (Figure 4B), longer total dendritic length (Figure 4C), and more dendritic branches at all developmental stages (Figure 4D), suggesting that *Lin28a* OE facilitated the development of new neurons.

To test whether LIN28A is necessary for the development of newborn neurons, we injected retrovirus expressing GFP-p2A-Cre into the DG of *Lin28a*$^{f/f}$ mice to knock out *Lin28a* from GFP$^+$ newborn DGCs (*Lin28a*$^{f/f}$), while Ctrl cells were labeled by retrovirus expressing GFP only (Figure 4E). At 3 wpi, we found that *Lin28a*$^{f/f}$ newborn DGCs showed less complex dendrites (Figure 4F), shorter dendritic length (Figure 4G), and less dendritic branches (Figure 4H).

Since the third week is a critical time period during which newborn DGCs form synapses with afferent glutamatergic projections (Kumamoto et al., 2012), we further analyzed the dendritic spines of the newborn DGCs at 3 wpi. We found that *Lin28a*-OE newborn DGCs exhibited greatly increased spine density, while *Lin28a*$^{f/f}$ newborn DGCs showed less spines (Figures 4I and 4J). We then did whole-cell recordings on labeled newborn DGCs and recorded the miniature excitatory postsynaptic currents (mEPSCs) at 3 wpi. We found that *Lin28a* OE in newborn neurons increased mEPSC frequency without affecting

Figure 4. LIN28A regulates the development and integration of newborn DGCs

(A) Images of newborn DGCs labeled by Ctrl or *Lin28a*-OE retroviruses at 1, 2, 3, and 4 wpi. Scale bar: 20 μm.

(B) Sholl analysis of newborn DGCs at 1, 2, 3, and 4 wpi.

(C) *Lin28a*-OE neurons showed longer total dendritic length (1 wpi: Ctrl N = 4 mice, n = 60 cells; *Lin28a*-OE N = 4 mice, n = 52 cells; ****p < 0.0001; 2 wpi: Ctrl N = 3 mice, n = 27 cells; *Lin28a*-OE N = 3 mice, n = 44 cells; ****p < 0.0001; 3 wpi: Ctrl N = 3 mice, n = 34 cells; *Lin28a*-OE N = 3 mice, n = 23 cells; ****p < 0.0001; 4 wpi: Ctrl N = 3 mice, n = 47 cells; *Lin28a*-OE N = 3 mice, n = 23 cells; ****p < 0.0001).

(D) *Lin28a*-OE neurons showed more dendritic branches (1 wpi: Ctrl N = 4 mice, n = 60 cells; *Lin28a-OE* N = 4 mice, n = 52 cells; ****p < 0.0001; 2 wpi: Ctrl N = 3 mice, n = 27 cells; *Lin28a-OE* N = 3 mice, n = 44 cells; *p = 0.0233; 3 wpi: Ctrl N = 3 mice, n = 34 cells; *Lin28a*-OE N = 3 mice, n = 23 cells; ****p < 0.0001; 4 wpi: Ctrl N = 3 mice, n = 47 cells; *Lin28a*-OE N = 3 mice, n = 23 cells; ****p < 0.0001).

(E) Images of 3 wpi neurons in *Lin28a*$^{f/f}$ mice labeled by retroviruses. Scale bar: 20 μm.

(F) Sholl analysis of newborn neurons at 3 wpi.

(G) *Lin28a*$^{f/f}$ neurons showed shorter total dendritic length (Ctrl N = 3 mice, n = 26 cells; *Lin28a*$^{f/f}$ N = 4 mice, n = 53 cells; ****p < 0.0001).

(H) *Lin28a*$^{f/f}$ neurons showed fewer dendritic branches (Ctrl N = 3 mice, n = 26 cells; *Lin28a*$^{f/f}$ N = 4 mice, n = 53 cells; ****p < 0.0001).

(I) Images showing dendritic spines of Ctrl or *Lin28a*-OE newborn DGCs (top) and Ctrl or *Lin28a*$^{f/f}$ newborn DGCs (bottom) at 3 wpi. Scale bar: 2 μm.

(J) Spine density in newborn DGCs at 3 wpi (C57 mice: Ctrl N = 3 mice, n = 30 dendritic segments; *Lin28a*-OE N = 3 mice, n = 30 dendritic segments; ****p < 0.0001; *Lin28a*$^{f/f}$ mice: Ctrl N = 3 mice, n = 22 dendritic segments; *Lin28a*$^{f/f}$ N = 3 mice, n = 18 dendritic segments; ****p < 0.0001).

(K) Representative traces of mEPSCs recorded from Ctrl and *Lin28a*-OE newborn DGCs at 3 wpi.

(L and M) Cumulative distribution of inter-event intervals and amplitude of mEPSCs in Ctrl and *Lin28a*-OE DGCs.

(N) Representative traces of mEPSCs recorded from Ctrl and *Lin28a*$^{f/f}$ neurons at 3 wpi.

(O and P) Cumulative distribution of inter-event intervals and amplitude of mEPSCs in Ctrl and *Lin28a*$^{f/f}$ neurons.

(Q) mEPSC frequency increased in *Lin28a*-OE neurons but decreased in *Lin28a*$^{f/f}$ neurons (C57 mice: Ctrl N = 3 mice, n = 12 neurons; *Lin28a*-OE N = 3 mice, n = 12 neurons; ***p = 0.0003; *Lin28a*$^{f/f}$ mice: Ctrl N = 3 mice, n = 9 neurons; *Lin28a*$^{f/f}$ N = 3 mice, n = 10 neurons; **p = 0.0027).

(R) mEPSC amplitude did not significantly change in *Lin28a*-OE or *Lin28a*$^{f/f}$ neurons (C57 mice: Ctrl N = 3 mice, n = 12 neurons; *Lin28a*-OE N = 3 mice, n = 12 neurons; p = 0.8257; *Lin28a*$^{f/f}$ mice: Ctrl N = 3 mice, n = 9 neurons; *Lin28a*$^{f/f}$ N = 3 mice, n = 10 neurons; p = 0.3119).

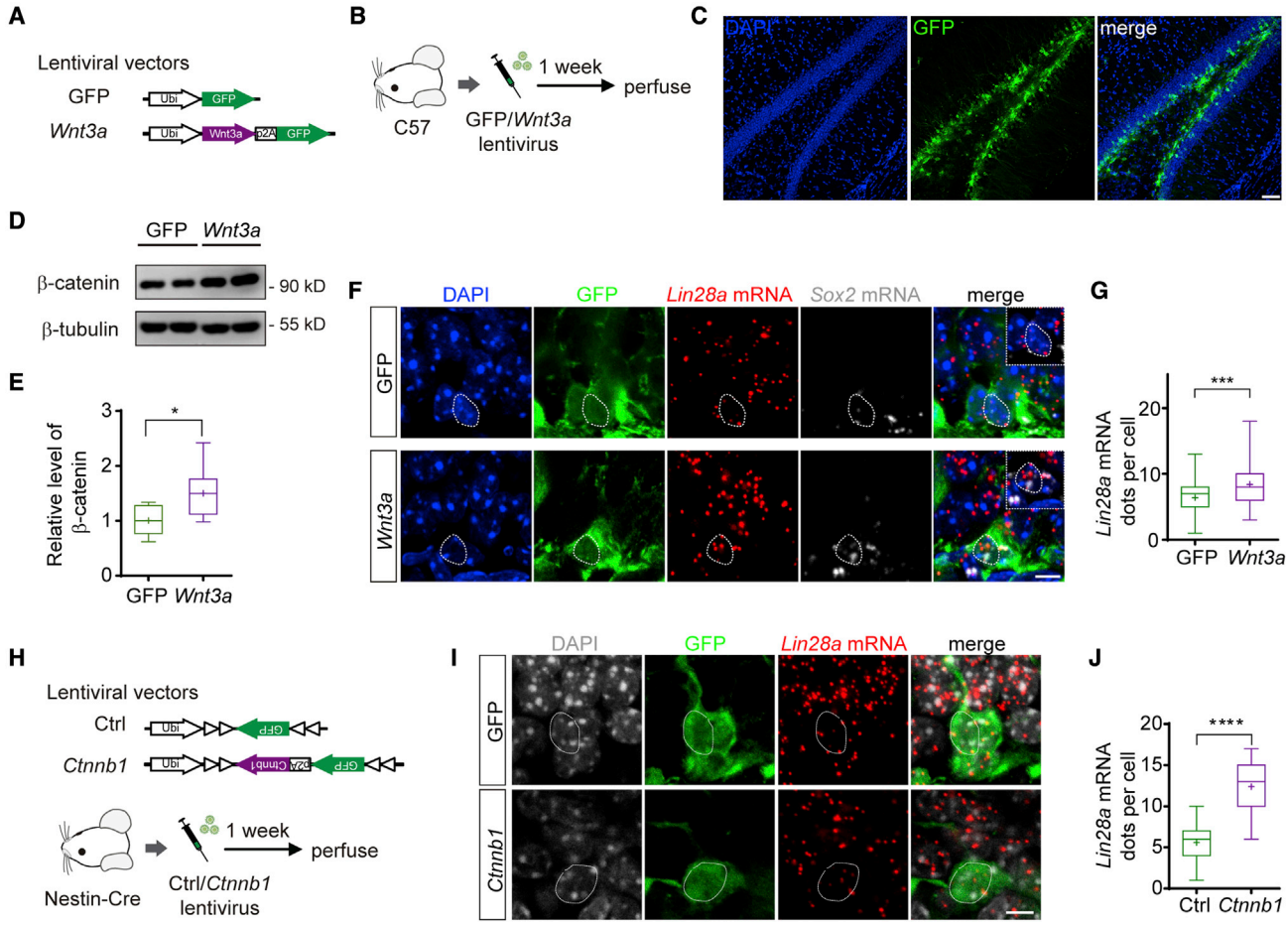

Figure 5. *Lin28a* expression in NPCs is regulated by Wnt/β-catenin signaling

(A) Schematics showing lentiviral vectors expressing GFP or *Wnt3a*.

(B) Experimental schematics.

(C) Images showing infection by *Wnt3a* lentivirus. Scale bar: 50 μm.

(D) Western blotting showing β-catenin level in the DG. β-tubulin was used as internal control.

(E) *Wnt3a* virus increased β-catenin in the DG (GFP n = 8 mice, *Wnt3a* n = 9 mice, *p = 0.0153).

(F) RNAscope images showing colocalization of *Lin28*a mRNA in *Sox2*-expressing NPCs (indicated by *Sox2* mRNA). Dotted lines outline the cell bodies of interested cells. Insets show the localization of *Lin28a* and *Sox2* mRNA around the nucleus (DAPI). Scale bar: 5 μm.

(G) *Wnt3a* virus increased *Lin28a* mRNA in *Sox2*-expressing NPCs (GFP: N = 3 mice, n = 56 cells; *Wnt3a*: N = 3 mice, n = 62 cells; ***p = 0.0001).

(H) Top: FLEX lentiviral vectors expressing GFP (Ctrl) or GFP-p2A-*Ctnnb1* (*Ctnnb1*). Bottom: experimental schematics.

(I) RNAscope images showing *Lin28a* mRNA in GFP-labeled NPCs. Scale bar: 5 μm.

(J) *Ctnnb1* OE increased *Lin28a* mRNA in NPCs (GFP: N = 3 mice, n = 63 cells; *Ctnnb1*: N = 3 mice, n = 37 cells; ****p < 0.0001).

mEPSC amplitude (Figures 4K–4M), whereas *Lin28a* KO reduced mEPSC frequency but not amplitude (Figures 4N–4R). Thus, these data suggest that *Lin28a* OE promoted, whereas *Lin28a* KO hindered, the development and functional integration of the newborn DGCs.

LIN28A was involved in the regulation of neurogenesis by Wnt signaling

Given that Wnt signaling regulates neurogenesis in the adult DG (Seib et al., 2013) and β-catenin promotes *Lin28a* expression in a variety of cell types (Cai et al., 2013; Yao et al., 2016), we wondered whether LIN28A acts as one of the downstream intracellular mechanisms of Wnt signaling. We injected lentivirus expressing *Wnt3a*, a Wnt agonist expressed in the hippocampal neurogenic niche (Kuwabara et al., 2009; Lie et al., 2005), into the DG of adult mice (Figures 5A–5C). We found that β-catenin in the DG increased (Figures 5D and 5E), suggesting an enhanced canonical Wnt signaling. Using RNAscope, we found the amount of *Lin28a* mRNA in

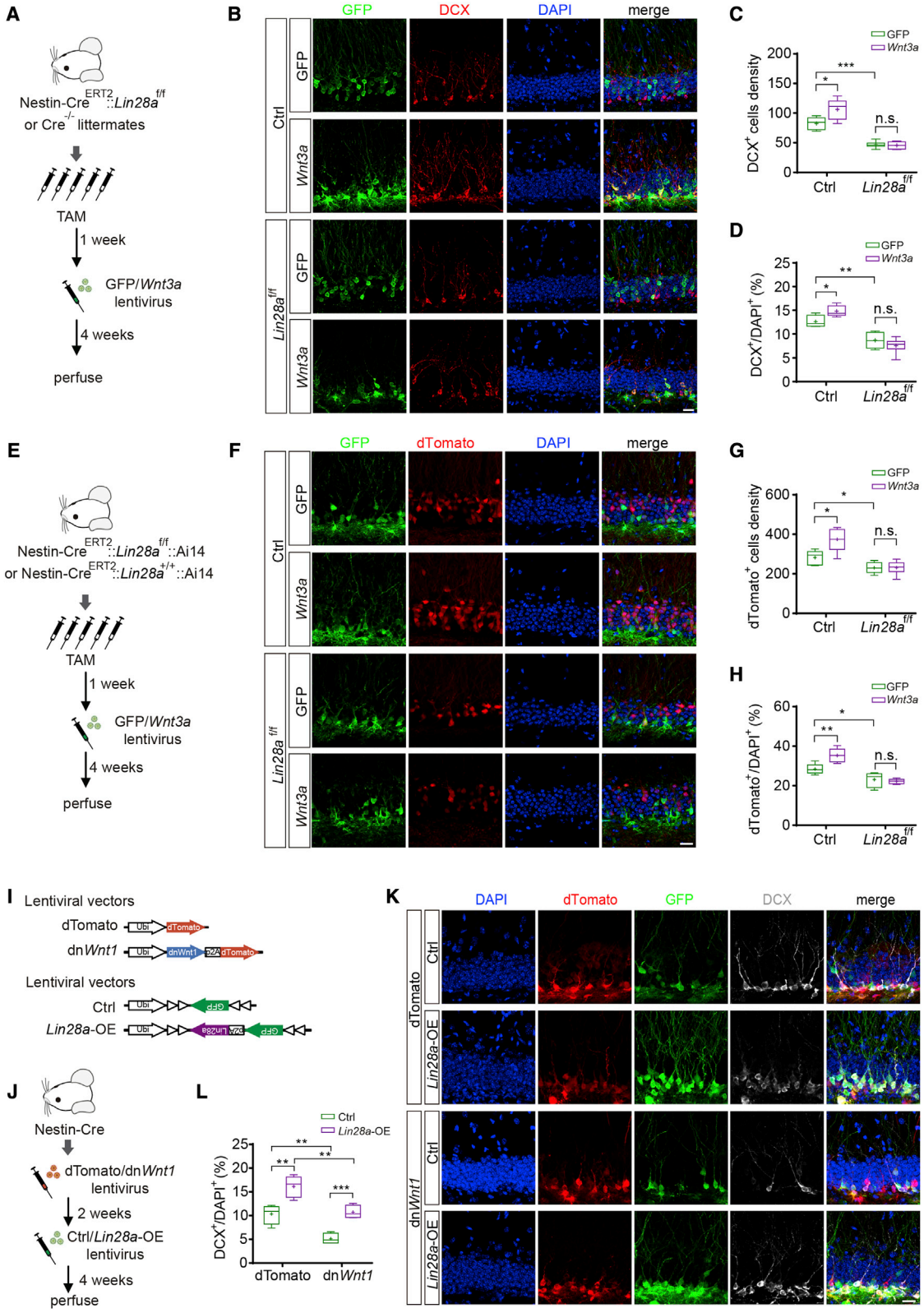

(legend on next page)

Sox2-expressing NPCs increased in *Wnt3a* mice compared with control mice (Figures 5F and 5G). These data suggest that *Lin28a* expression in NPCs was increased by enhanced Wnt signaling.

To further confirm that the upregulation of β-catenin directly enhanced *Lin28a* expression, we injected FLEX lentivirus expressing mouse *Ctnnb1*, which codes the protein β-catenin (Figure 5H), into the DG of Nestin-Cre mice and performed RNAscope a week later. We found that *Ctnnb1* OE in NPCs indeed increased the mRNA level of *Lin28a* in the labeled cells (Figures 5I and 5J). Furthermore, applying SKL2001, a Wnt/β-catenin agonist (Gwak et al., 2012), increased the level of β-catenin (Figures S6A and S6B) and enhanced *Lin28a* expression (Figure S6C) in cultured mouse hippocampal neurons. To further confirm whether β-catenin could bind to specific sites in the *Lin28a* promoter region, we performed a chromatin immunoprecipitation (ChIP) assay using a β-catenin antibody with cell lysates from cultured mouse hippocampal neurons. Compared with a randomly selected -1.5 kb region (R1), quantitative real-time PCR results showed specific binding of endogenous β-catenin to the -0.5 (R2) and -0.15 kb (R3) regions upstream of *Lin28a* gene (Figures S6D and S6E). These results suggest that β-catenin could indeed bind to the *Lin28a* promoter region and activate *Lin28a* expression in neurons.

Next, to examine whether *Lin28a* KO in NPCs could block the pro-neurogenic effects of Wnt ligands, we injected lentivirus expressing *Wnt3a* into the DG of Nestin-Cre^{ERT2}::*Lin28a*$^{f/f}$ mice 1 week after TAM administration (Figure 6A), by which *Lin28a* was knocked out from Nestin^{+} NPCs (*Lin28a*$^{f/f}$). Four more weeks later, we found that *Wnt3a* OE increased DCX^{+} cells in Cre$^{-/-}$ littermates (Ctrl). In contrast, enhancing *Wnt3a* expression did not increase DCX^{+} cells in *Lin28a*$^{f/f}$ mice (Figures 6B–6D). To confirm this finding, we next used Nestin-Cre^{ERT2}::*Lin28a*$^{f/f}$::Ai14 mice to label the progenies of the NPCs lacking *Lin28a* (*Lin28a*$^{f/f}$); Nestin-Cre^{ERT2}::*Lin28a*$^{+/+}$::Ai14 mice of the same age were used as Ctrl (Figure 6E). Consistently, we found that *Wnt3a* OE increased dTomato^{+} cells in control mice but not in *Lin28a*$^{f/f}$ mice (Figures 6F–6H). These results indicate that LIN28A in NPCs was necessary for the regulation of neurogenesis by niche Wnt ligands.

Deficiency in Wnt signaling results in decreased neurogenesis in the adult DG (Jang et al., 2013; Seib et al., 2013). To test whether *Lin28a* OE is sufficient to recover impaired neurogenesis in Wnt-deficient hippocampus, we constructed a lentiviral vector expressing a dominant negative *Wnt1* (dn*Wnt1*) (Figure 6I) to inhibit Wnt signaling (Choi et al., 2018; Lie et al., 2005). We injected lentivirus expressing dn*Wnt1*-dTomato or dTomato only into Nestin-Cre mice and infused lentivirus expressing FLEX GFP-p2A-*Lin28a* (Figure 6I) 2 weeks later to overexpress *Lin28a* in NPCs (using FLEX-GFP as Ctrl) (Figure 6J). Four more weeks later, we found that dn*Wnt1* decreased DCX^{+} cells in the DG, whereas *Lin28a* OE in NPCs increased DCX^{+} cells in dTomato mice and recovered DCX^{+} cells in dn*Wnt1* mice (Figures 6K and 6L). These data suggest that *Lin28a* OE in NPCs was sufficient to restore neurogenesis in Wnt-deficient neurogenic niche.

Lin28a OE in NPCs restores neurogenesis in the aging hippocampus and enhances pattern separation

Since *Lin28a* OE could increase NPC proliferation and facilitate the integration of newborn DGCs, we wondered

Figure 6. LIN28A is involved in the regulation of neurogenesis by Wnt

(A) Experimental schematics.

(B) DCX^{+} newborn DGCs in Ctrl or *Lin28a*$^{f/f}$ mice. Scale bar: 20 μm.

(C) *Wnt3a* virus increased DCX^{+} cell in Ctrl mice but not in *Lin28a*$^{f/f}$ mice (Ctrl: GFP n = 4 mice, *Wnt3a* n = 5 mice; *p = 0.0379; *Lin28a*$^{f/f}$: GFP n = 6 mice, *Wnt3a* n = 6 mice; p = 0.7054; Ctrl GFP versus *Lin28a*$^{f/f}$ GFP, ***p = 0.0002).

(D) *Wnt3a* virus increased the percentage of DCX^{+} cell in the GCL in Ctrl mice but not in *Lin28a*$^{f/f}$ mice (Ctrl: GFP n = 4 mice, *Wnt3a* n = 5 mice; *p = 0.0299; *Lin28a*$^{f/f}$: GFP n = 6 mice, *Wnt3a* n = 6 mice; p = 0.2918; Ctrl GFP versus *Lin28a*$^{f/f}$ GFP, **p = 0.0047).

(E) Experimental schematics.

(F) Images showing dTomato^{+} newborn DGCs. Scale bar: 20 μm.

(G) *Wnt3a* increased the density of dTomato^{+} DGCs in Ctrl mice, but not in *Lin28a*$^{f/f}$ mice (Ctrl: GFP n = 5 mice, *Wnt3a* n = 5 mice; *p = 0.0193; *Lin28a*$^{f/f}$: GFP n = 6 mice, *Wnt3a* n = 6 mice; p = 0.9700; Ctrl GFP versus *Lin28a*$^{f/f}$ GFP, *p = 0.0242).

(H) *Wnt3a* increased the percentage of dTomato^{+} DGCs in Ctrl mice but not in *Lin28a*$^{f/f}$ mice (Ctrl: GFP n = 5 mice, *Wnt3a* n = 5 mice; **p = 0.0077; *Lin28a*$^{f/f}$: GFP n = 6 mice, *Wnt3a* n = 6 mice; p = 0.5659; Ctrl GFP versus *Lin28a*$^{f/f}$ GFP, *p = 0.0238).

(I) Lentiviral vectors expressing dTomato or dn*Wnt1* (top) and FLEX lentiviral vectors expressing GFP (Ctrl) or GFP-p2A-*Lin28a* (*Lin28a*-OE) (bottom).

(J) Experimental schematics.

(K) Images showing DCX^{+} newborn neurons. Scale bar: 20 μm.

(L) dn*Wnt1* decreased the percentage of DCX^{+} DGCs, whereas *Lin28a* OE recovered the number of DCX^{+} cells (dTomato: Ctrl n = 4 mice, *Lin28a*-OE n = 5 mice; **p = 0.0052; dn*Wnt1*: Ctrl n = 4 mice, *Lin28a*-OE n = 4 mice; ***p = 0.0008; dTomato Ctrl versus dn*Wnt1* Ctrl, **p = 0.0045; dTomato *Lin28a*-OE versus dn*Wnt1* *Lin28a*-OE, **p = 0.0041).

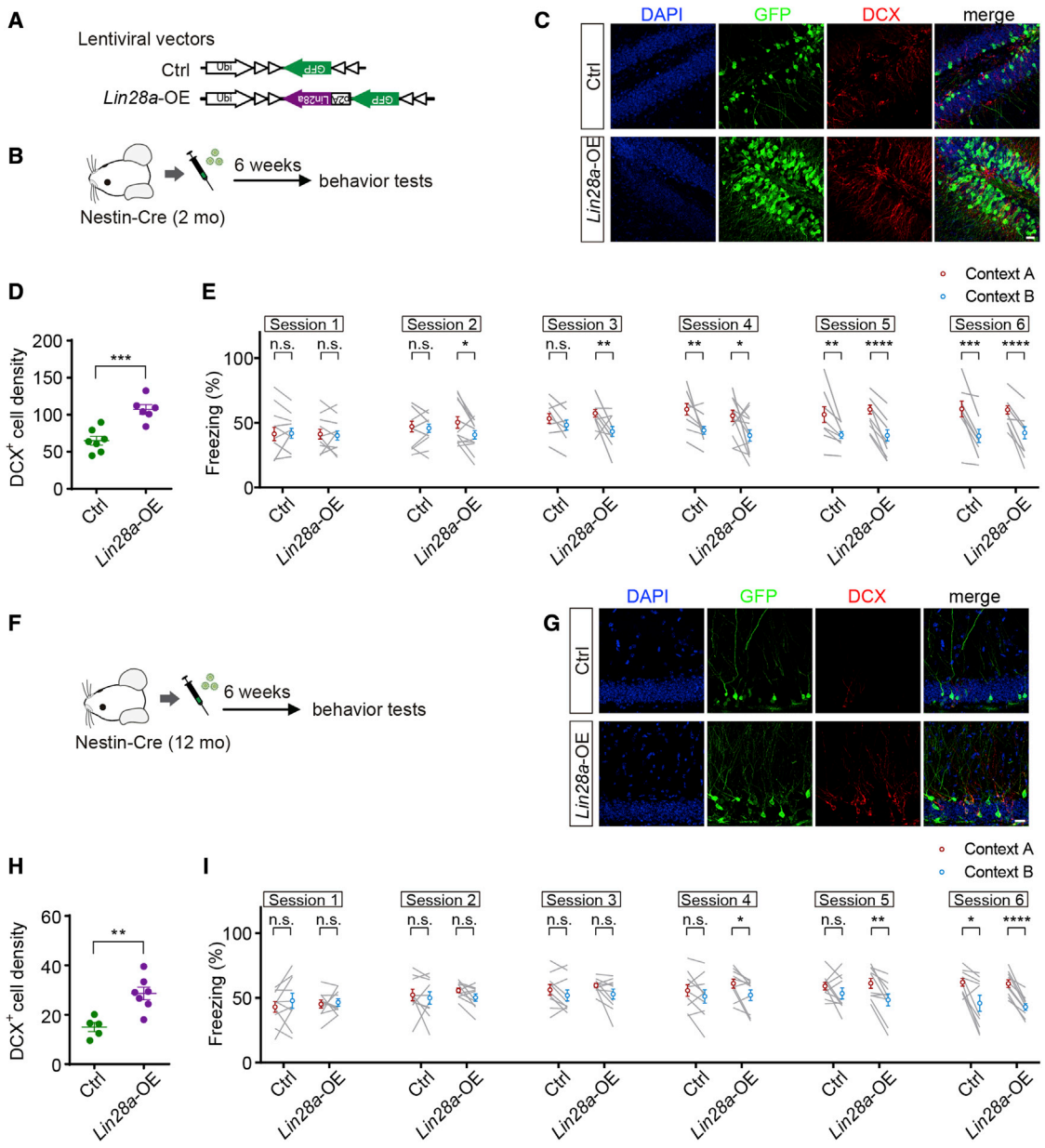

Figure 7. *Lin28a* OE in hippocampal NPCs increases neurogenesis and enhances pattern separation

(A) FLEX lentiviral vectors.

(B) Experimental schematics.

(C) Images showing DCX$^+$ cells in the DG. Scale bar: 20 μm.

(D) Density of DCX$^+$ cells (Ctrl n = 7 mice, *Lin28a*-OE n = 6 mice, ***p = 0.0005).

(E) Freezing of mice in contexts A and B in test sessions 1 through 6 (Ctrl n = 13 mice, *Lin28a*-OE n = 13 mice; two-tailed paired t test; session 1: Ctrl p = 0.8661, *Lin28a*-OE p = 0.6783; session 2: Ctrl p = 0.6152, *Lin28a*-OE *p = 0.0128; session 3: Ctrl p = 0.0648, *Lin28a*-OE **p = 0.0088; session 4: Ctrl **p = 0.0033, *Lin28a*-OE *p = 0.0295; session 5: Ctrl **p = 0.0020, *Lin28a*-OE ****p < 0.0001; session 6: Ctrl ***p = 0.0002, *Lin28a*-OE ****p < 0.0001).

(F) Experimental schematics.

(G) Images showing DCX$^+$ cells in the DG of aging mice. Scale bar: 20 μm.

(H) Density of DCX$^+$ cells (Ctrl n = 5 mice, *Lin28a*-OE n = 7 mice; **p = 0.0026).

(legend continued on next page)

whether *Lin28a* OE could enhance pattern separation by increasing hippocampal neurogenesis. We injected lentivirus expressing FLEX GFP-p2A-*Lin28a* (*Lin28a*-OE) into the DG of 2-month-old (2 mo) Nestin-Cre mice to overexpress *Lin28a* in a large population of existing NPCs (GFP as Ctrl) (Figures 7A and 7B). Six weeks later, *Lin28a*-OE mice showed increased DCX^+ cells compared with Ctrl mice (Figures 7C and 7D). Meanwhile, *Lin28a*-OE mice discriminated contexts A and B in session 2, while Ctrl mice showed discrimination in session 4 (Figure 7E), suggesting that *Lin28a*-OE mice exhibited enhanced pattern separation.

To test whether *Lin28a* OE could enhance the neurogenesis and improve pattern separation in aging mice, we injected the viruses in 12-month-old (12 mo) Nestin-Cre mice (Figure 7F). Six weeks later, we found *Lin28a* OE increased DCX^+ cells in the DG of aging mice compared with Ctrl mice (Figures 7G and 7H). Consistently, the aging mice in the Ctrl group exhibited poor pattern separation, as they did not discriminate the two contexts till session 6 (Figure 7I). Interestingly, *Lin28a*-OE aging mice discriminated contexts A and B in session 4, suggesting a restored ability of pattern separation (Figure 7I).

Additionally, *Lin28a* OE in hippocampal NPCs in young (2-months-old) and aging (12-months-old) mice did not alter their performance in single-trial CFC (Figure S7A), NOR (Figure S7B), or OF tests (Figure S7C). Interestingly, *Lin28a* OE enhanced the NLR in young, but not aging, mice (Figure S7D), suggesting the rejuvenation of hippocampal neurogenesis by *Lin28a* OE was limited by the remaining NPC pool.

DISCUSSION

LIN28A regulates neurogenesis in the adult hippocampus

During early brain development, *Lin28* is highly expressed in NPCs (Yang et al., 2015). Interestingly, our results showed that LIN28A remained existent in NPCs and DGCs in the adult hippocampus. Loss of *Lin28a* in hippocampal NPCs decreased neurogenesis, whereas *Lin28a* OE increased neurogenesis by enhancing NPC proliferation, in agreement with a previous study that *Lin28a* KO in the developing brain results in microcephaly whereas *Lin28a* OE leads to enlarged brain (Yang et al., 2015). Our results also showed that *Lin28a* OE in NPCs enhanced neurogenesis mainly by increasing cell cycles and expanding $TBR2^+$ intermediate progenitor cells. Further analysis showed that *Lin28a* OE decreased the newborn cell differentiated towards astrocytes, consistent with a previous report showing that LIN28 suppresses glial fate of NPCs *in vitro* (Balzer et al., 2010).

As an RNA-binding protein, LIN28A represses *let-7* miRNA biogenesis, thus regulating multiple signaling pathways and the expression of numerous genes (Jun-Hao et al., 2016; Shyh-Chang and Daley, 2013; Zhu et al., 2011). Our data showed that an anti-*let-7* sponge increased the proliferation of NPCs and their progenies, mimicking the effects of *Lin28a* OE. This suggests the involvement of the Lin28a/*let-7* pathway in regulating neurogenesis in the adult DG, consistent with a previous study on retinal Müller cells (Yao et al., 2016). However, LIN28A has also been reported to directly bind to mRNAs such as *cyclin A/B* and *Igf2* and thus regulate cell cycle, differentiation, and cellular growth independently of *let-7* (Balzer et al., 2010; Shyh-Chang and Daley, 2013). Since we cannot rule out the possibility that the *let-7*-independent pathways may also be involved in the regulation of neurogenesis by LIN28A, further studies will be needed.

In addition, *Lin28a* KO inhibited, while *Lin28a* OE facilitated, the development and functional integration of newborn DGCs, suggesting that LIN28A controls neuronal growth. However, a recent study showed that *Lin28* OE in the SVZ NPCs decreased the number of new neurons in the olfactory bulb of postnatal mice (Romer-Seibert et al., 2019). This result may be attributed to the fact that the increased LIN28 repressed *let-7*, which is important for the migration of neuroblasts (Petri et al., 2017), thus decreasing the number of new neurons arriving in the olfactory bulb.

Decrease of *Lin28a* expression is involved in aging-associated decline of neurogenesis

Hippocampal neurogenesis decreases in mammals with aging (Kuhn et al., 1996; Spalding et al., 2013), associated with and contributing to cognitive declines (Lee et al., 2012; Seib et al., 2013). The Wnt signaling pathway is essentially important in regulating multiple stages of adult neurogenesis (Lie et al., 2005; Schafer et al., 2015). Existing in the neurogenic niche and changing with age or activity, Wnt ligands promote (Lie et al., 2005; Song et al., 2002), while Wnt antagonists inhibit, neurogenesis (Jang et al., 2013; Seib et al., 2013). Increasing evidence shows that the reduced Wnt ligands and the increased Wnt antagonists in the hippocampal niche are associated with aging

(I) Freezing of mice in contexts A and B in test sessions 1 through 6 (Ctrl n = 10 mice, *Lin28a*-OE n = 10 mice; two-tailed paired t test; session 1: Ctrl p = 0.3203, *Lin28a*-OE p = 0.7178; session 2: Ctrl p = 0.6352, *Lin28a*-OE p = 0.0620; session 3: Ctrl p = 0.1426, *Lin28a*-OE p = 0.0792; session 4: Ctrl p = 0.2146, *Lin28a*-OE *p = 0.0237; session 5: Ctrl p = 0.2287, *Lin28a*-OE **p = 0.0040; session 6: Ctrl *p = 0.0106, *Lin28a*-OE ****p < 0.0001).

(Bayod et al., 2015; Miranda et al., 2012; Okamoto et al., 2011; Seib et al., 2013), resulting in decreased Wnt signaling activity (Bayod et al., 2015; Heppt et al., 2020).

Coincidently, *Lin28a* expression in the DG decreased with aging. We found that LIN28A regulated the proliferation of NPCs and the development of new neurons. Especially, *Lin28a* KO reduced neurogenesis and inhibited the development of new DGCs, mimicking the effects of reduced Wnt/β-catenin activity (Jang et al., 2013; Miranda et al., 2012; Okamoto et al., 2011; Seib et al., 2013), whereas *Lin28a* OE increased the proliferation of NPCs and promoted the development of newborn DGCs, consistent with the increased neurogenesis by enhanced Wnt/β-catenin activity (Heppt et al., 2020; Lie et al., 2005). Importantly, *Lin28a* KO in NPCs blocked the enhanced neurogenesis by WNT3A, suggesting that LIN28A is essential for NPCs to respond to local Wnt agonists. On the other hand, blocking Wnt signaling decreased neurogenesis, which could be rescued by *Lin28a* OE in NPCs. Consistently, in aging animals, *Lin28a* OE in the remaining NPCs could at least partially restore hippocampal neurogenesis.

Furthermore, we found that enhancing Wnt/β-catenin signaling increased *Lin28a* expression both *in vivo* and *in vitro*. Using a ChIP assay, we found that endogenous β-catenin could bind to specific regions upstream of the *Lin28a* gene in neurons, in agreement with previous studies (Cai et al., 2013; Yao et al., 2016).

These data suggest that *Lin28a* expression is directly regulated by Wnt/β-catenin signaling and that LIN28A serves as a downstream mechanism underlying the regulation of neurogenesis by niche Wnt signals. Thus, in the aging brain, with reduced Wnt signaling activity (Heppt et al., 2020; Seib et al., 2013), decreased LIN28A may contribute to the declining neurogenesis.

Adult hippocampal neurogenesis is important for hippocampus-dependent cognitions, such as pattern separation (Nakashiba et al., 2012; Sahay et al., 2011a). *Lin28a* KO resulted in decreased neurogenesis, associated with impaired pattern separation, decreased NLR, and heightened anxiety levels, recapitulating the phenotypes in the aging mice. *Lin28a* OE in NPCs increased neurogenesis in both young and aging mice, depending on the remaining pool of NPCs, thus enhancing their pattern separation. In these animals, we did not observe significant change in the anxiety level, possibly because the diffusion of the injected virus was limited in the dorsal DG (Gu et al., 2012), while leaving the ventral DG unaffected, which is more related to anxiety regulation (Kheirbek et al., 2013). In addition, mounting evidence has shown that Wnt signaling modulates synaptic plasticity and regulates formation of dendritic spines in neurons (McLeod and Salinas, 2018; Narvaes and Furini, 2022), which are crucial for memory formation and storage. Our previous study has demonstrated that *Lin28a* KO decreased the long-term potentiation (LTP) in mature DGCs and impaired spatial memory (Hu et al., 2021). These clues suggest that the reduced LIN28A in neurons may also contribute to the cognitive decline in aging mice in addition to decreasing hippocampal neurogenesis.

Taken together, our study revealed that LIN28A regulates neurogenesis in response to Wnt signaling in the adult hippocampus, suggesting that the reduced LIN28A acts as one important link between the changes in niche Wnt ligands/antagonists and the decreased neurogenesis in the aging brain, and is associated with impaired cognition. As other target genes of Wnt/β-catenin signaling through LEF/TCF, such as *Neurod1* and *Prox1*, have also been shown to regulate neurogenesis (Gao et al., 2009; Kuwabara et al., 2009; Lavado et al., 2010; Lie et al., 2005; Miranda et al., 2012), further studies will be needed to understand possible interactions between these molecules.

EXPERIMENTAL PROCEDURES

Animals

All procedures were approved by the Animal Care and Use Committees at Zhejiang University School of Medicine and were conducted in accordance with the policies of institutional guidelines on the care and use of laboratory animals. All mice were maintained at a 12 h light/dark cycle and group housed (3–4 per cage) with free access to normal food and water.

Lin28a$^{f/f}$ mice (stock no. 023913), Nestin-Cre mice (stock no. 003771), Nestin-Cre^{ERT2} mice (stock no. 016261), and Ai14 reporter line (stock no. 007914) were from Jackson Labs, and Nestin-GFP mice (stock no. RBRC06355) were from RIKEN.

TAM administration

TAM (Sigma, T5648) was dissolved in vegetable oil containing 0.1% absolute ethanol to a concentration of 100 mg/mL. To knock out *Lin28a* from Nestin^{+} NPCs in Nestin-Cre^{ERT2}::*Lin28a*$^{f/f}$ mice or Nestin-Cre^{ERT2}::*Lin28a*$^{f/f}$::Ai14 mice, TAM was administered intraperitoneally (i.p.) at a dose of 160 mg/kg every 3 days for 5 times.

Plasmid construction and virus production

The coding sequences (CDSs) of genes were synthesized and subcloned into retroviral or lentiviral plasmid vectors. Plasmids were then co-transfected to 293T cells with helper plasmids for retrovirus or lentivirus using Lipofectamine 2000 (Invitrogen). Culture medium was collected, and virus was purified and concentrated by ultracentrifugation.

Virus injection

Stereotactic viral injections were performed in accordance with the Guidelines by Zhejiang University Animal Care and Use Committees. As previously described (Gu et al., 2012), mice were anesthetized using isoflurane, and viral particles were injected

stereotaxically into the DG. Mice were returned to their home cages after waking up and then housed under standard conditions.

Immunostaining, confocal imaging, and image analysis

As previously described (Gu et al., 2012), mice were deeply anesthetized and perfused transcardially with PBS and then 4% PFA. Brains were removed, fixed overnight in PFA, and then transferred to a 30% (w/v) sucrose solution and stored at 4°C. Brains were sectioned, stained, and imaged. Images were then analyzed using Image J or Imaris (see supplemental experimental procedures for details).

RNAscope *in situ* hybridization

In situ hybridization was performed using RNAscope multiplex fluorescent reagent kit (Advanced Cell Diagnostics) according to manufacturer's instructions. Sections were then imaged, and images were analyzed using ImageJ.

Whole-cell electrophysiological recordings

Acute brain sections were made 3 weeks after retroviral injection, and electrophysiological recordings were performed at 32°C–34°C, as previously described (Gu et al., 2012). Briefly, mice were deeply anesthetized with isoflurane, brain was removed, and acute brain slices were prepared. GFP-labeled neurons were identified under fluorescent microscope, and whole-cell patch-clamp recordings were performed. mEPSCs were recorded in the presence of tetrodotoxin (1 μM) and picrotoxin (100 μM) at a holding potential of -70 mV. Miniature events were automatically detected and then analyzed using Clampfit software.

Behavior procedures for CFC and pattern-separation tests

Mice were placed in a conditioning chamber containing a stainless-steel shock-grid floor (context A) for 2 min and then received a single foot shock (0.75 mA, 2 s duration). Mice were taken out of the chamber 1 min after the foot shock and placed back into their home cages. After training, mice were housed under standard conditions until the test. The freezing of the mice was tested in context A on the following day. The animals were continuously trained in context A with foot shock and context B without foot shock for another 11 consecutive days for the pattern-separation tests.

Statistical analysis

Data were analyzed using GraphPad Prism 8.0 software. Statistical analysis was carried out using two-tailed unpaired t tests unless otherwise indicated. For analyzing cell-cluster size, two-tailed unpaired t tests were performed for the average clonal size, following Kolmogorov-Smirnov tests for the cumulative distributions. For the statistical analysis of the animals' freezing in the pattern-separation tests, paired t tests were used to analyze the difference of the animals' freezing in contexts A and B in the same session. Data were presented using box-and-whisker plots or scatter plots. For box-and-whisker plots, whiskers represent the minimum and maximum, the boxes represent the upper and lower quartiles, the line in the middle represents the median, and the "+" represents the mean. For the scatter plots, data are presented as the mean ± SEM. Statistical significance was considered when $p < 0.05$.

SUPPLEMENTAL INFORMATION

Supplemental information can be found online at https://doi.org/10.1016/j.stemcr.2022.05.016.

AUTHOR CONTRIBUTIONS

Z.H., Lang Wang, and Y.G. designed all the experiments; Z.H. conducted most of the experiments, including most plasmid construction, viral injection, imaging, electrophysiology, and behavioral experiments; J.M. and Y.L. did virus production, RNAscope, real-time PCR, ChIP, and western blots; H.Y. constructed XFP plasmid vectors and some imaging; X.L. and C.W. did some imaging and analysis; Liang Wang provided the Ai14 mouse line; B.S. provided the Nestin-Cre and Nestin-GFP mouse lines; Z.C. provided the Nestin-Cre^{ERT2} mouse line; and Z.H., J.M., Lang Wang, and Y.G. discussed the results and wrote the manuscript. All authors read and discussed about the manuscript.

ACKNOWLEDGMENTS

This work was supported by the National Key R&D Program of China (2017YFA0104200), the Zhejiang Provincial Natural Science Foundation of China (LR17C090001), the National Natural Science Foundation of China (32071021), and startup funds to Y.G. and the National Natural Science Foundation of China (32070975) and the Zhejiang Provincial Natural Science Foundation of China (LR21C090001) to Lang Wang. We are grateful to the Core Facilities of Zhejiang University School of Medicine for technical assistance.

CONFLICTS OF INTEREST

The authors declare that they have no conflicts of interest.

Received: January 7, 2022
Revised: May 21, 2022
Accepted: May 23, 2022
Published: June 23, 2022

REFERENCES

Anacker, C., and Hen, R. (2017). Adult hippocampal neurogenesis and cognitive flexibility - linking memory and mood. Nat. Rev. Neurosci. *18*, 335–346. https://doi.org/10.1038/nrn.2017.45.

Balzer, E., Heine, C., Jiang, Q., Lee, V.M., and Moss, E.G. (2010). LIN28 alters cell fate succession and acts independently of the let-7 microRNA during neurogliogenesis in vitro. Development *137*, 891–900. https://doi.org/10.1242/dev.042895.

Bayod, S., Felice, P., Andrés, P., Rosa, P., Camins, A., Pallàs, M., and Canudas, A.M. (2015). Downregulation of canonical Wnt signaling in hippocampus of SAMP8 mice. Neurobiol. Aging *36*, 720–729. https://doi.org/10.1016/j.neurobiolaging.2014.09.017.

Cai, W.Y., Wei, T.Z., Luo, Q.C., Wu, Q.W., Liu, Q.F., Yang, M., Ye, G.D., Wu, J.F., Chen, Y.Y., Sun, G.B., et al. (2013). The Wnt-beta-catenin pathway represses let-7 microRNA expression through

transactivation of Lin28 to augment breast cancer stem cell expansion. J. Cell Sci. *126*, 2877–2889. https://doi.org/10.1242/jcs.123810.

Choi, S.H., Bylykbashi, E., Chatila, Z.K., Lee, S.W., Pulli, B., Clemenson, G.D., Kim, E., Rompala, A., Oram, M.K., Asselin, C., et al. (2018). Combined adult neurogenesis and BDNF mimic exercise effects on cognition in an Alzheimer's mouse model. Science *361*, eaan8821. https://doi.org/10.1126/science.aan8821.

Christian, K.M., Song, H., and Ming, G.L. (2014). Functions and dysfunctions of adult hippocampal neurogenesis. Annu. Rev. Neurosci. *37*, 243–262. https://doi.org/10.1146/annurev-neuro-071013-014134.

Cimadamore, F., Amador-Arjona, A., Chen, C., Huang, C.T., and Terskikh, A.V. (2013). SOX2-LIN28/let-7 pathway regulates proliferation and neurogenesis in neural precursors. Proc. Natl. Acad. Sci. U. S. A *110*, E3017–E3026. https://doi.org/10.1073/pnas.1220176110.

Gao, Z., Ure, K., Ables, J.L., Lagace, D.C., Nave, K.A., Goebbels, S., Eisch, A.J., and Hsieh, J. (2009). Neurod1 is essential for the survival and maturation of adult-born neurons. Nat. Neurosci. *12*, 1090–1092. https://doi.org/10.1038/nn.2385.

Gonçalves, J.T., Schafer, S.T., and Gage, F.H. (2016). Adult neurogenesis in the Hippocampus: from stem cells to behavior. Cell *167*, 897–914. https://doi.org/10.1016/j.cell.2016.10.021.

Gu, Y., Arruda-Carvalho, M., Wang, J., Janoschka, S.R., Josselyn, S.A., Frankland, P.W., and Ge, S. (2012). Optical controlling reveals time-dependent roles for adult-born dentate granule cells. Nat. Neurosci. *15*, 1700–1706. https://doi.org/10.1038/nn.3260.

Gwak, J., Hwang, S.G., Park, H.S., Choi, S.R., Park, S.H., Kim, H., Ha, N.C., Bae, S.J., Han, J.K., Kim, D.E., et al. (2012). Small molecule-based disruption of the Axin/beta-catenin protein complex regulates mesenchymal stem cell differentiation. Cell Res. *22*, 237–247. https://doi.org/10.1038/cr.2011.127.

Heppt, J., Wittmann, M.T., Schaffner, I., Billmann, C., Zhang, J., Vogt-Weisenhorn, D., Prakash, N., Wurst, W., Taketo, M.M., and Lie, D.C. (2020). β-catenin signaling modulates the tempo of dendritic growth of adult-born hippocampal neurons. EMBO J. *39*, e104472. https://doi.org/10.15252/embj.2020104472.

Hu, Z.C., Ma, J., and Gu, Y. (2021). Lin28a is essential for synaptic plasticity in dentate granule cells and spatial memory. Neurosci. Bull. *37*, 261–266. https://doi.org/10.1007/s12264-020-00591-7.

Jang, M.H., Bonaguidi, M.A., Kitabatake, Y., Sun, J., Song, J., Kang, E., Jun, H., Zhong, C., Su, Y., Guo, J.U., et al. (2013). Secreted frizzled-related protein 3 regulates activity-dependent adult hippocampal neurogenesis. Cell Stem Cell *12*, 215–223. https://doi.org/10.1016/j.stem.2012.11.021.

Jun-Hao, E.T., Gupta, R.R., and Shyh-Chang, N. (2016). Lin28 and let-7 in the metabolic physiology of aging. Trends Endocrinol. Metabol. *27*, 132–141. https://doi.org/10.1016/j.tem.2015.12.006.

Kheirbek, M.A., Drew, L.J., Burghardt, N.S., Costantini, D.O., Tannenholz, L., Ahmari, S.E., Zeng, H., Fenton, A.A., and Hen, R. (2013). Differential control of learning and anxiety along the dorsoventral axis of the dentate gyrus. Neuron *77*, 955–968. https://doi.org/10.1016/j.neuron.2012.12.038.

Kuhn, H.G., Dickinson-Anson, H., and Gage, F.H. (1996). Neurogenesis in the dentate gyrus of the adult rat: age-related decrease of neuronal progenitor proliferation. J. Neurosci. *16*, 2027–2033. https://doi.org/10.1523/jneurosci.16-06-02027.1996.

Kumamoto, N., Gu, Y., Wang, J., JenoSchka, S., Takemaru, K., Levine, J., and Ge, S. (2012). A role for primary cilia in glutamatergic synaptic integration of adult-born neurons. Nat. Neurosci. *15*, 399–405. https://doi.org/10.1186/2046-2530-1-s1-p31.

Kuwabara, T., Hsieh, J., Muotri, A., Yeo, G., Warashina, M., Lie, D.C., Moore, L., Nakashima, K., Asashima, M., and Gage, F.H. (2009). Wnt-mediated activation of NeuroD1 and retro-elements during adult neurogenesis. Nat. Neurosci. *12*, 1097–1105. https://doi.org/10.1038/nn.2360.

Lavado, A., Lagutin, O.V., Chow, L.M.L., Baker, S.J., and Oliver, G. (2010). Prox1 is required for granule cell maturation and intermediate progenitor maintenance during brain neurogenesis. PLoS Biol. *8*, e1000460. https://doi.org/10.1371/journal.pbio.1000460.

Lee, S.W., Clemenson, G.D., and Gage, F.H. (2012). New neurons in an aged brain. Behav. Brain Res. *227*, 497–507. https://doi.org/10.1016/j.bbr.2011.10.009.

Lie, D.C., Colamarino, S.A., Song, H.J., Désiré, L., Mira, H., Consiglio, A., Lein, E.S., Jessberger, S., Lansford, H., Dearie, A.R., et al. (2005). Wnt signalling regulates adult hippocampal neurogenesis. Nature *437*, 1370–1375. https://doi.org/10.1038/nature04108.

McLeod, F., and Salinas, P.C. (2018). Wnt proteins as modulators of synaptic plasticity. Curr. Opin. Neurobiol. *53*, 90–95. https://doi.org/10.1016/j.conb.2018.06.003.

Ming, G.L., and Song, H. (2011). Adult neurogenesis in the mammalian brain: significant answers and significant questions. Neuron *70*, 687–702. https://doi.org/10.1016/j.neuron.2011.05.001.

Miranda, C.J., Braun, L., Jiang, Y., Hester, M.E., Zhang, L., Riolo, M., Wang, H., Rao, M., Altura, R.A., and Kaspar, B.K. (2012). Aging brain microenvironment decreases hippocampal neurogenesis through Wnt-mediated survivin signaling. Aging Cell *11*, 542–552. https://doi.org/10.1111/j.1474-9726.2012.00816.x.

Nakashiba, T., Cushman, J.D., Pelkey, K.A., Renaudineau, S., Buhl, D.L., McHugh, T.J., Rodriguez Barrera, V., Chittajallu, R., Iwamoto, K.S., McBain, C.J., Fanselow, M., and Tonegawa, S. (2012). Young dentate granule cells mediate pattern separation, whereas old granule cells facilitate pattern completion. Cell *149*, 188–201. https://doi.org/10.1016/j.cell.2012.01.046.

Narvaes, R.F., and Furini, C.R.G. (2022). Role of Wnt signaling in synaptic plasticity and memory. Neurobiol. Learn. Mem. *187*, 107558. https://doi.org/10.1016/j.nlm.2021.107558.

Ngwenya, L.B., Heyworth, N.C., Shwe, Y., Moore, T.L., and Rosene, D.L. (2015). Age-related changes in dentate gyrus cell numbers, neurogenesis, and associations with cognitive impairments in the rhesus monkey. Front. Syst. Neurosci. *9*, 102. https://doi.org/10.3389/fnsys.2015.00102.

Okamoto, M., Inoue, K., Iwamura, H., Terashima, K., Soya, H., Asashima, M., and Kuwabara, T. (2011). Reduction in paracrine Wnt3 factors during aging causes impaired adult neurogenesis. FASEB J. *25*, 3570–3582. https://doi.org/10.1096/fj.11-184697.

Petri, R., Pircs, K., Jönsson, M.E., Akerblom, M., Brattas, P.L., Klussendorf, T., and Jakobsson, J. (2017). let-7 regulates radial migration of new-born neurons through positive regulation of autophagy. EMBO J. *36*, 1379–1391. https://doi.org/10.15252/embj.201695235.

Romer-Seibert, J.S., Hartman, N.W., and Moss, E.G. (2019). The RNA-binding protein LIN28 controls progenitor and neuronal cell fate during postnatal neurogenesis. FASEB J. *33*, 3291–3303. https://doi.org/10.1096/fj.201801118r.

Sahay, A., Scobie, K.N., Hill, A.S., O'Carroll, C.M., Kheirbek, M.A., Burghardt, N.S., Fenton, A.A., Dranovsky, A., and Hen, R. (2011a). Increasing adult hippocampal neurogenesis is sufficient to improve pattern separation. Nature *472*, 466–470. https://doi.org/10.1038/nature09817.

Sahay, A., Wilson, D.A., and Hen, R. (2011b). Pattern separation: a common function for new neurons in hippocampus and olfactory bulb. Neuron *70*, 582–588. https://doi.org/10.1016/j.neuron.2011.05.012.

Schafer, S.T., Han, J., Pena, M., von Bohlen Und Halbach, O., Peters, J., and Gage, F.H. (2015). The Wnt adaptor protein ATP6AP2 regulates multiple stages of adult hippocampal neurogenesis. J. Neurosci. *35*, 4983–4998. https://doi.org/10.1523/jneurosci.4130-14.2015.

Seib, D.R., Corsini, N.S., Ellwanger, K., Plaas, C., Mateos, A., Pitzer, C., Niehrs, C., Celikel, T., and Martin-Villalba, A. (2013). Loss of Dickkopf-1 restores neurogenesis in old age and counteracts cognitive decline. Cell Stem Cell *12*, 204–214. https://doi.org/10.1016/j.stem.2012.11.010.

Shyh-Chang, N., and Daley, G.Q. (2013). Lin28: primal regulator of growth and metabolism in stem cells. Cell Stem Cell *12*, 395–406. https://doi.org/10.1016/j.stem.2013.03.005.

Sierra, A., Encinas, J.M., Deudero, J.J., Chancey, J.H., Enikolopov, G., Overstreet-Wadiche, L.S., Tsirka, S.E., and Maletic-Savatic, M. (2010). Microglia shape adult hippocampal neurogenesis through apoptosis-coupled phagocytosis. Cell Stem Cell *7*, 483–495. https://doi.org/10.1016/j.stem.2010.08.014.

Song, H., Stevens, C.F., and Gage, F.H. (2002). Astroglia induce neurogenesis from adult neural stem cells. Nature *417*, 39–44. https://doi.org/10.1038/417039a.

Spalding, K.L., Bergmann, O., Alkass, K., Bernard, S., Salehpour, M., Huttner, H.B., Bostrom, E., Westerlund, I., Vial, C., , et al.Buchholz, B.A. (2013). Dynamics of hippocampal neurogenesis in adult humans. Cell *153*, 1219–1227. https://doi.org/10.1016/j.cell.2013.05.002.

Yang, M., Yang, S.L., Herrlinger, S., Liang, C., Dzieciatkowska, M., Hansen, K.C., Desai, R., Nagy, A., Niswander, L., Moss, E.G., et al. (2015). Lin28 promotes the proliferative capacity of neural progenitor cells in brain development. Development *142*, 1616–1627. https://doi.org/10.1242/dev.120543.

Yang, X., Rutnam, Z.J., Jiao, C., Wei, D., Xie, Y., Du, J., Zhong, L., and Yang, B.B. (2012). An anti-let-7 sponge decoys and decays endogenous let-7 functions. Cell Cycle *11*, 3097–3108. https://doi.org/10.4161/cc.21503.

Yao, K., Qiu, S., Tian, L., Snider, W.D., Flannery, J.G., Schaffer, D.V., and Chen, B. (2016). Wnt regulates proliferation and neurogenic potential of müller glial cells via a Lin28/let-7 miRNA-dependent pathway in adult mammalian retinas. Cell Rep. *17*, 165–178. https://doi.org/10.1016/j.celrep.2016.08.078.

Zhu, H., Shyh-Chang, N., Segrè, A., Shinoda, G., Shah, S.P., Einhorn, W.S., Takeuchi, A., Engreitz, J.M., Hagan, J.P., Kharas, M.G., et al. (2011). The Lin28/let-7 axis regulates glucose metabolism. Cell *147*, 81–94. https://doi.org/10.1016/j.cell.2011.08.033.